PAPER AAS 95-341

Issues Concerning East-West Stationkeeping of Satellite Orbits with Resonant Tesseral Harmonics

T. A. Ely and K. C. Howell

School of Aeronautics and Astronautics
Purdue University
West Lafayette, IN 47907-1282
(317) 494-5139

AAS/AIAA Astrodynamics Specialist Conference

HALIFAX, NOVA SCOTIA, CANADA 14–17 AUGUST 1995

AAS Publications Office, P.O. Box 28130, San Diego, CA 92198

AAS 95-341

ISSUES CONCERNING EAST-WEST STATIONKEEPING OF ORBITS WITH RESONANT TESSERAL HARMONICS

Todd A. Ely[†] and Kathleen C. Howell[#]

Eccentric and inclined orbits with near-repeating groundtracks represent a class of orbits that is dynamically complex. Deep resonance with the Earth's tesseral harmonics may result in satellite trajectories that are chaotic. Because of the interaction between tesseral harmonics, neighboring chaotic trajectories diverge exponentially over time from each other. This paper describes potential modifications to traditional East-West stationkeeping approaches to maintain orbits that are eccentric and regular. Consideration is then given to chaotic orbits; under certain conditions, variations of perigee over time can destabilize the control process. Analytic criteria for predicting the likelihood of this divergence are developed. Additionally, potential strategies for overcoming the instability, as well as mission planning issues, are discussed.

Introduction

Eccentric and inclined orbits with near-repeating groundtracks result in satellite trajectories that return to the same region periodically throughout the day and spend a majority of the flight time over one hemisphere of the Earth. Unlike more benign geostationary orbits, this class of synchronous orbits is dynamically very complex. In this orbital regime, geopotential tesseral harmonics can interact to produce multiple resonances that result in significant nonlinear motions compared to nearby orbits without resonances. In a previous paper, the authors[1] demonstrate that as an orbit's eccentricity grows, the resonance islands associated with individual long-period tesseral (longitude dependent) geopotential harmonics increase in size and begin to interact. Eventually, the resonance islands overlap and break up invariant tori originally lying between them, thus producing regions of chaos. Furthermore, at the 'critical' inclination another resonance with zonal (longitude independent) geopotential harmonics must be considered. At this value of inclination, the tesserals and long-period zonal harmonics overlap to produce regions of chaos, as well.[2]

This study presents a preliminary investigation into East-West stationkeeping for eccentric, resonant orbits that are regular or chaotic. The classical method for East-West stationkeeping (or 'longitude control') utilizes a deadband around a nominal stroboscopic mean node. The control strategy uses targeting burns at one node boundary to force the trajectory to drift and graze the other boundary. The trajectory then drifts back towards the starting node, where the cycle is repeated. This method has been investigated by many authors, including Gedeon[3], Kamel, et al.[4], and Chao and Schmitt.[5] However, these previous investigators only consider regular (or integrable) orbits, typically with near zero eccentricities. In the present study, the same method is considered for eccentric orbits that can exhibit chaotic responses. Using Poincaré sections, chaotic regions of phase space are identified. The sections provide insight not only into the natural evolution of an orbit, but into the stability of the stationkeeping method, as well. Analytical and numerical results show that the stationkeeping method can be unstable in the chaotic region, thus, indicating the need to further investigate this problem including alternate control approaches. Again, using the Poincaré sections, a potential method is proposed. To illustrate these concepts, 24 hr and 12 hr resonant orbits with significant eccentricities and inclinations are the focus of this effort. Additionally, resonance overlap at critical inclination is considered. To avoid drag

[†] Graduate Student, School of Aeronautics and Astronautics, Purdue University, 1282 Grissom Hall, West Lafayette, Indiana 47907-1282.

[#] Associate Professor, School of Aeronautics and Astronautics, Purdue University, 1282 Grissom Hall, West Lafayette, Indiana 47907-1282.

perturbations the selected range of orbits remains beyond the Earth's atmosphere; eccentricities below .73 prove sufficient.

Model Formulation

For the orbits considered here, the selected gravity model employs a specialized version of the Kaula[6] geopotential expansion. The analysis considers the long term evolution of the mean elements, hence short periodic terms are ignored. The model includes the point mass inverse square term, the first order secular oblateness term, and critical long period tesseral harmonic terms. When critical inclination orbits are considered, the second order long period oblateness term is included, as well. The Hamiltonian associated with this dynamical model can be written in the form,

$$H = -\frac{\mu}{2a} + V_{J_2^2} + \sum_{l,m,p,q} V_{lmpq}(a,e,i,\Omega,\omega,M,\theta_e). \tag{1}$$

The form of the second order oblateness term $V_{J_2^2}$ is,

$$V_{J_2^2} = -\frac{\mu}{a^5}\frac{R_e^4 J_2^2}{4}\left[A(a,e,i)\cos 2\omega + C(a,e,i)\right]. \tag{2}$$

The detailed expressions for A and C are discussed by Hough[7] and Delhaise[2]. An individual tesseral harmonic term V_{lmpq} is represented as,

$$V_{lmpq} = -\frac{\mu R_e^l}{a^{l+1}} F_{lmp}(i) G_{lpq}(e) J_{lm} \cos\psi_{lmpq}(\Omega,\omega,M,\theta_e) \equiv h_{lmpq}(a,e,i)\cos\psi_{lmpq}(\Omega,\omega,M,\theta_e). \tag{3}$$

The classical orbital elements (a,e,i,Ω,ω,M) produce a 6 dimensional (6-D) phase space; μ is the Earth's reduced mass, R_e is the Earth radius, θ_e is the mean Greenwich sidereal angle, $F_{lmp}(i)$ and $G_{lpq}(e)$ are the inclination and eccentricity functions, respectively, defined in [6], and $J_{lm} = \sqrt{C_{lm}^2 + S_{lm}^2}$ is the unnormalized coefficient corresponding to the tesseral harmonic of degree l and order m. Note that $G_{lpq}(e)$ is written explicitly as a power series and, in the subsequent analysis, terms to the order $O(e^{44})$ are retained. This is consistent with a first order analysis, and the range of eccentricities investigated. A note on evaluating the function $G_{lpq}(e)$ is in order. In subsequent analysis it is found that the essential features of the dynamics can be discerned from only 3 to 5 harmonic terms. Because this is a small number, the authors employ an explicit expansion of $G_{lpq}(e)$ (obtained by symbolic manipulation using *Mathematica*®) rather than implementing a recursive formulation. For the purposes of the present paper, this approach is more efficient. The angle argument represents the following function,

$$\psi_{lmpq} = (l-2p+q-\frac{m}{s})(M+\omega) + m\left\{\frac{1}{s}(M+\omega) - (\theta_e - \Omega) - \lambda_{lm}\right\} - q\omega, \tag{4}$$

and,

$$\lambda_{lm} = \begin{cases} \frac{1}{m}\tan^{-1}\left(\frac{S_{lm}}{C_{lm}}\right) & l-m \text{ even} \\ \frac{1}{m}\tan^{-1}\left(\frac{C_{lm}}{-S_{lm}}\right) & l-m \text{ odd} \end{cases}, \tag{5}$$

where λ_{lm} is the phase angle associated with J_{lm}, and s is the integer nearest the ratio: satellite mean motion over Earth rotation rate. The expansion terms have a variety of characteristic time scales that decompose into identifiable secular, short period, and long period effects. For the 24 hr and 12 hr orbits, the primary secular terms result from Earth's oblateness (the V_{2010} zonal term and its associated second order term), and the long period terms are due to critical (or resonant) tesseral terms (V_{lmpq}) and the second order oblateness term. The critical tesseral harmonics are found by retaining terms in Eq. (1) that have angular rates $\dot{\psi}_{lmpq}$ near zero. This results in the following condition on the expansion indices,

$$l - 2p + q - \frac{m}{s} = 0. \tag{6}$$

The expression in Eq. (4) reduces to $\psi_{lmpq} = m(\lambda - \lambda_{lm}) - q\omega$ where,

$$\lambda \equiv \frac{1}{s}(M + \omega) - (\theta_e - \Omega), \tag{7}$$

is the stroboscopic mean node, often called the mean longitude in the 24 hr case. Applying the condition in Eq. (6) to the 24 hr and 12 hr resonant orbits yields the critical harmonics used in the analysis, and are listed in Table 1. Other critical harmonics exist, but those in Table 1 are the primary resonance terms that affect the qualitative nature of the motion. Also note that the 24 hr harmonic terms $V_{2200}, V_{3110}, V_{3300}$ are grouped together because they have the same angular rate.

Table 1

PRIMARY CRITICAL HARMONICS FOR THE 12 HR AND 24 HR RESONANT ORBITS

12 hr Orbits	V_{220-1}	V_{3210}	V_{2211}
24 hr Orbits	$V_{2200}, V_{3110}, V_{3300}$	V_{3211}	V_{2212}

The resulting nonlinear model, represented in the form,

$$H = -\frac{\mu}{2a} + V_{2010} + \sum_{\Re} V_{lmpq}, \tag{8}$$

contains the primary dynamical features that are required for determining resonant, long term orbit evolution. The finite set $\Re$ contains the critical harmonics involved in the summation, including the second order oblateness term. The Hamiltonian in Eq. (8) is transformed into action/angle coordinates by introducing the Delaunay elements $(L, G, H, l, g, h) = ((\mu a)^{1/2}, L(1-e^2)^{1/2}, G\cos i, M, \omega, \Omega)$. An additional transformation using the following generating function,

$$F_2 = \lambda I_1 + \omega I_2 + \Omega I_3 = \left\{ \frac{1}{s}(M+\omega) - (\theta_e t + \theta_{eo} - \Omega) \right\} I_1 + \omega I_2 + \Omega I_3, \tag{9}$$

reduces the system by one degree of freedom. The resulting Hamiltonian can be rewritten formally as,

$$\begin{aligned} H &= H_o(I_1, I_2) + \varepsilon H_1(I_1, I_2, \lambda, \omega) \\ &= -\frac{\mu^2}{2L^2} - s\dot{\theta}_e L + V_{2010}(L(I_1), e(I_1, I_2), i(I_1, I_2, I_3)) + \sum_{\Re} V_{lmpq}(L(I_1), e(I_1, I_2), i(I_1, I_2, I_3), \lambda, \omega). \end{aligned} \tag{10}$$

Because Ω does not appear in the argument list of Eq. (10), its associated action $I_3 = L(1-e^2)^{1/2}\cos i - sL$ is ignorable and constant. The Hamiltonian in Eq. (10) now represents an autonomous 2-DOF system (versus nonautonomous 3-DOF) with actions $I_1 = sL$, $I_2 = L(1-e^2)^{1/2} - L$ and associated angles λ, ω, respectively. Note that the original variables L, e, i prove more convenient for use in later manipulations than the current actions, therefore the functional dependency on L, e, i will be carried. The integrable portion of the vector field H_o includes the inverse square and secular terms. The perturbation εH_1 includes the critical resonant harmonic terms that perturb the integrable field, and may eliminate the integrability of the system.

Overview of Classical East-West Stationkeeping

A resonant satellite in a nearly circular orbit has a phase space that is reducible to 1-DOF. The phase variables in this problem are the action $I_1 = sL$ (or, equivalently, semi-major axis) and the stroboscopic mean node λ. Near the exact resonance the satellite 'librates' around a stable fixed point and further away the satellite 'circulates' around the Earth. An example of this response is shown in Figure 1 for a geostationary orbit. In most cases, the node varies by a significant amount, one that is typically larger than the desired range, so, to maintain a nearly constant node, some form of nodal control is required. The traditional method utilizes the libration cycles to maximize the drift time between control maneuvers. A sample 'drift cycle' is depicted in Figure 1. The satellite trajectory is maintained within a deadband region $\Delta\lambda$ that is centered around a desired nominal node λ_n. The cycle begins at point 1 where the trajectory drifts from the deadband's lower node boundary λ_l; then grazes the upper node boundary λ_u; and, finally, returns to λ_l. At point 2 a maneuver is implemented to lower the semi-major axis to point 1, where the cycle repeats. The size of the maneuver depends on the nominal node location and the size of the deadband.

The classical stationkeeping method can be employed to control satellite orbits that are in resonance with an isolated tesseral harmonic V_{lmpq} (such as V_{2200} for geostationary orbits). Consider the circular orbit case, $e = 0$; this implies that $q = 0$ and the angle argument in Eq. (10) is a function only of the node λ. A 'local' Hamiltonian for this system can be determined by expanding the action variable around its exact resonance location for the harmonic, and retaining terms of order $O(J_{lm})$. The condition for exact resonance is $\dot{\lambda} = 0$. For a given eccentricity e^* and inclination i^*, its solution produces a value of L^* (or a^*). The equations of motion that result from this Hamiltonian are,

$$\delta\dot{L} = J_{lm}\frac{m}{s}\frac{\mu^{l+2}R_e^l}{L^{*2l+2}}\left|F_{lmp}(i^*)G_{lpq}(e^*)\right|\sin\left[m(\lambda-\lambda_{lm})\right], \tag{11a}$$

$$\dot{\lambda} = -\frac{3}{s}\frac{\mu^2}{L^{*4}}\delta L, \tag{11b}$$

where $\delta L = L - L^* = O(J_{lm}^{1/2})$, and the angle is shifted by π if $F_{lmp}(i^*)G_{lpq}(e^*) > 0$. The nodal acceleration is obtained by differentiating Eq. (11b) with respect to time and substituting the resulting expression into Eq. (11a), that yields,

$$\begin{aligned}\ddot{\lambda} &= -3J_{lm}\frac{m}{s^2}\frac{\mu^{l+4}R_e^l}{L^{*2l+6}}\left|F_{lmp}(i^*)G_{lpq}(e^*)\right|\sin\left[m(\lambda-\lambda_{lm})\right], \\ &= -3mJ_{lm}\left(\frac{n}{s}\right)^2\left(\frac{R_e}{a^*}\right)^l\left|F_{lmp}(i^*)G_{lpq}(e^*)\right|\sin\left[m(\lambda-\lambda_{lm})\right]\end{aligned} \tag{12}$$

Typically, a stationkeeping deadband region $\Delta\lambda$ is less than 4° in width or $O(10^{-2})$, thus, for time spans that are short relative to the libration period, the acceleration can be considered a constant. Holding the node fixed at the nominal value λ_n, Eq. (12) can be integrated immediately to produce an equation that is quadratic in time, that is,

$$\lambda = \lambda_1 + \dot{\lambda}_1(t-t_1) + \ddot{\lambda}\frac{(t-t_1)^2}{2}, \tag{13}$$

where the 1 refers to conditions at point 1 in Figure 1. The cycle is symmetric about the exact resonance value a^* therefore $\dot{\lambda}_2 = -\dot{\lambda}_1$ ($\Rightarrow a_2 = -a_1$). Also, the boundary condition for grazing is represented by the resonance equation $\dot{\lambda}(t_g) = 0$ where t_g is the time of grazing (halfway through the drift cycle). Using these conditions the cycle parameters can be determined. The time between maneuvers is,

$$\Delta t = 2\sqrt{2\left|\frac{\Delta\lambda}{\ddot{\lambda}}\right|}, \tag{14}$$

and the change in nodal rate (or semi-major axis) is,

$$\Delta\dot{\lambda} = 2\dot{\lambda}_2 = \pm 2\sqrt{2\left|\ddot{\lambda}\Delta\lambda\right|} \quad \Rightarrow \quad \Delta a = \mp\frac{4sa}{3n}\sqrt{2\left|\ddot{\lambda}\Delta\lambda\right|}, \tag{15}$$

where $\Delta\dot{\lambda} > 0$ when $\ddot{\lambda} < 0$, and $\Delta\dot{\lambda} < 0$ when $\ddot{\lambda} > 0$. To minimize the impact on other elements, the maneuver is performed at perigee. This results in a change to both eccentricity and semi-major axis, but not to any other elements. The expressions for the maneuver cost and eccentricity change are,

$$\Delta v = \frac{n}{2}\sqrt{\frac{1-e^*}{1+e^*}}\Delta a \quad \text{and} \quad \Delta e = \frac{(1-e^*)}{a^*}\Delta a. \tag{16a,b}$$

The fundamental assumptions associated with this approach include a nodal acceleration that remains constant during a cycle, and a cycle that is symmetric about the resonance location. In the following discussions, regions of the phase space in which these fundamental assumptions cease to be valid are

identified using the Poincaré sections. The next section also includes modifications to the traditional stationkeeping method to adjust for eccentric orbits.

East-West Stationkeeping of Eccentric Orbits

Development. When an orbit is eccentric, additional tesseral harmonic terms are introduced into the equations of motion (the governing Hamiltonian in Eq. (10)). Unlike Eqs. (11), however, the angular arguments now include terms in which q is nonzero, and, thus, they are functions of both the node and perigee. First consider orbits below critical inclination, i.e., perigee is secular. Again, expand the Hamiltonian to first order around the exact resonance location defined by the condition $\dot{\lambda} = 0$,

$$\delta\dot{L} = -\frac{1}{s}\left\{ \sum_{\Re,q=0} m h^*_{lmpq} \sin[m(\lambda - \lambda_{lm})] + \sum_{\Re,q\neq 0} m h^*_{lmpq} \sin[m(\lambda - \lambda_{lm}) - q\omega(t)] \right\}, \tag{17a}$$

$$\dot{\lambda} = \frac{1}{s}\frac{\partial^2 H_o}{\partial L^{*2}}\delta L, \tag{17b}$$

$$\dot{\omega} \equiv \dot{\omega}_{sec} = \frac{\partial H_o}{\partial I_2} = \frac{3J_2\mu^3 R_e^2}{L^{*7}\left(1-e^{*2}\right)}\left(2 - \frac{5}{2}\sin^2 i^*\right). \tag{17c}$$

Note that the coefficients in Eq. (17a) are constant, and the second derivative in Eq. (17b) is constant and includes the inverse square and secular terms. The perigee rate is of order $O(J_2) = O(J_{lm}^{1/2})$ when the inclination is below the critical value, however at critical inclination Eqs. (17b,c) must be modified to include the second order J_2 term. Proceeding as before, fix the node to its nominal value λ_n. The harmonic terms with $q = 0$ can be considered constant, however the terms with $q \neq 0$ are explicitly time dependent because of perigee. The time dependence invalidates the two fundamental assumptions in the classical stationkeeping method: the nodal acceleration is not guaranteed to have a constant sign within a cycle, and the element time histories are not symmetric around the exact resonance value.

Failure of the symmetry condition implies that the targeting of the grazing node $\lambda(t_g)$ is now accomplished as a numerical two point boundary value problem (TPBVP). Failure of the constant nodal acceleration assumption implies that the stationkeeping process can be unstable. First consider the TPBVP, and note that for small variations in the node and secular changes in perigee, the equations of motion can be integrated analytically from the starting condition, with the resulting form,

$$\delta L - \delta L_1 = -\frac{1}{s}\left\{ \sum_{\Re,q=0} mh^*_{lmpq} \sin[m\Delta\phi_{lm}](t-t_1) + \sum_{\Re,q\neq 0} \frac{mh^*_{lmpq}}{q\dot{\omega}_{sec}} \left(\cos[m\Delta\phi_{lm} - q\omega(t)] - \cos[m\Delta\phi_{lm} - q\omega_1]\right) \right\}, \quad (18a)$$

$$\lambda - \lambda_1 = -\frac{1}{s^2}\frac{\partial^2 H_o}{\partial L^{*2}}\left\{ \sum_{\Re,q=0} mh^*_{lmpq} \sin[m\Delta\phi_{lm}] \frac{(t-t_1)^2}{2} - \left(\delta L_1 + \sum_{\Re,q\neq 0} \frac{mh^*_{lmpq}}{q\dot{\omega}_{sec}} \cos[m\Delta\phi_{lm} - q\omega_1] \right)(t-t_1) - \right.$$
$$\left. \sum_{\Re,q\neq 0} \frac{mh^*_{lmpq}}{(q\dot{\omega}_{sec})^2} \left(\sin[m\Delta\phi_{lm} - q\omega(t)] - \sin[m\Delta\phi_{lm} - q\omega_1]\right) \right\}, \quad (18b)$$

where $\Delta\phi_{lm} = \lambda_n - \lambda_{lm}$. For a given deadband $\Delta\lambda$, the unknowns in Eqs. (18) are $\delta L_1, \delta L_2, t_g$, and t_2, and the boundary conditions remain as $\lambda_1 = \lambda_2, \lambda(t_g) \equiv \lambda_g = \lambda_1 + \Delta\lambda$, and $L(t_g) = 0$. The appearance of trigonometric functions prevents a simple analytical solution for these equations. Thus, in order to simulate stationkeeping for eccentric orbits that have a secular dependence on perigee, numerical targeting techniques are necessary. A simple method for this targeting proceeds as follows:

i) Use the analytical result from Eq. (15) and Eq. (17b) to determine a first guess for δL_1.

ii) Propagate till either the boundary is crossed $\left(\lambda = \lambda_g\right)$, or the nodal rate passes through exact resonance $\left(\dot{\lambda} = 0 \Rightarrow \delta L = 0\right)$.

iii) Use simple variations derived from Eq. (13), (assume $\ddot{\lambda}$ and t_g are constant) and Eq. (17b) to iterate δL_1:

a) $\lambda = \lambda_g, \dot{\lambda}(t_g^i) = \dot{\lambda}_g^i \neq 0$: $\quad \delta L_1^{i+1} = \delta L_1^i - s\zeta \left(\frac{\partial^2 H_o}{\partial L^{*2}} \right) \dot{\lambda}_g^i,$ (19a)

b) $\lambda(t_g^i) = \lambda_g^i \neq \lambda_g, \dot{\lambda}_g = 0$: $\quad \delta L_1^{i+1} = \delta L_1^i + s\zeta \left(\frac{\partial^2 H_o}{\partial L^{*2}} \right) \left(\frac{\lambda_g - \lambda_g^i}{t_g^i - t_1} \right),$ (19b)

where the index i refers to the current iteration value, and ζ is an attenuation factor to accommodate neglected nonlinearities and variations in t_g.

iv) After convergence to the grazing boundary conditions, determine the cost (Δv) using Eq. (16a); propagate forward until the node returns to the current value; then repeat the cycle.

The stability issue can be addressed by considering the nature of the fixed points of the integrable problem with an isolated harmonic, Eqs. (11). The fixed points produce either elliptic centers or hyperbolic saddle points. The hyperbolic saddle points are connected by a separatrix, with no other solution connecting these points. This follows from uniqueness of solutions and that the system is 2-dimensional (2-D). Thus, a system typically librates or circulates depending on the initial conditions. The phase plane is similar to that in Figure 1. The present situation is markedly different, because, with the introduction of perigee, the phase space becomes 3-D. Of course, solutions remain unique in the 3-D space, however, now a trajectory may pass through a point on the original 2-D phase plane more than once. This makes it possible for a trajectory that is restricted in node and semi-major axis now to have several dynamic responses over time. The stability of the stationkeeping process just described is

predicated on the action rate (or nodal acceleration) having a nearly constant value. Instabilities can occur if the action rate passes through zero and changes sign. The potential for this condition exists if the coefficients h^*_{lmpq} in the second summation of Eq. (17a) are sufficiently large.

A useful tool for assessing stability of a planar projection of the phase space is the Poincaré section. For the problems considered in this paper, the section provides complete information on the regular or chaotic nature of the system. Consider the Poincaré section of the integrable problem with an isolated harmonic sampled at returns to a specified value of perigee; again, the resulting plot is similar to that in Figure 1. The libration and circulation orbits lie on invariant KAM surfaces. Now, as other harmonic terms increase in size (i.e., when eccentricity increases) they perturb the original KAM surfaces. According to the KAM Theorem, if the perturbation is sufficiently small and far from resonance, then the surfaces deform, but remain $O(\varepsilon)$-close to the original unperturbed surfaces. Thus, libration (or circulation) orbits that satisfy the conditions of the KAM theorem are perturbed to similar libration (or circulation) orbits. Furthermore, if a segment of an unperturbed libration orbit is defined such that the action rate is not equal to zero, then the action rate along the corresponding perturbed segment is not equal to zero. Therefore, the preceding stationkeeping method remains convergent on libration curve segments that persist under perturbation. However, the theorem does not address surfaces that bifurcate to produce more complex quasiperiodic motions, or break up to yield regions of chaos. It is possible that perturbed orbits lying in these dynamically complex regions can encounter zero action rates, and, thus, destabilize the stationkeeping process. Indeed, this is demonstrated in later simulations. Fortunately, for 2-degree of freedom systems, the Poincaré section can provide a complete depiction of where KAM curves persist under perturbation, and, additionally, where they do not. Thus, a section provides a useful visual tool to assess the likelihood of instability.

Passage through a value of the action rate equal to zero can be explicitly predetermined by selecting specific initial conditions. In Eq. (17a), retain the harmonics present at all eccentricities ($q = 0$), as well as the two neighboring harmonics ($q = \pm 1$), then set the equation equal to zero,

$$\sum_{\Re,q=0} mh^*_{lmpq} \sin[m\Delta\phi_{lm}] + mh^*_{lmpq} \sin[m\Delta\phi_{lm} - \omega(t)] + mh^*_{lmpq} \sin[m\Delta\phi_{lm} + \omega(t)] = 0. \tag{20}$$

Solving for $\omega(t)$ yields,

$$\left\{\omega(t_{z_1}), \omega(t_{z_2})\right\} = \left\{\cos^{-1}(\alpha) + \beta,\ 2\pi - \cos^{-1}(\alpha) + \beta\right\}, \tag{21}$$

where,

$$\alpha = -\left(\frac{\sum_{\Re,q=0} mh^*_{lmpq} \sin[m\Delta\phi_{lm}]}{\sqrt{\left(h^{*2}_{lmp-1} + h^{*2}_{lmp+1}\right) + \left(h^{*2}_{lmp-1} - h^{*2}_{lmp+1}\right)}} \right), \quad \tan\beta = \frac{\left(h^*_{lmp-1} - h^*_{lmp+1}\right)\cos m\Delta\phi_{lm}}{\left(h^*_{lmp-1} + h^*_{lmp+1}\right)\sin m\Delta\phi_{lm}}. \tag{22a,b}$$

If the harmonic coefficients associated with $q \neq 0$ are sufficiently large, then $|\alpha| < 1$, and the system will encounter a zero. Otherwise, $|\alpha| > 1$ and the ω are undefined, and the system encounters no zeros. To compute the times until encounter with the perigee values determined by Eq. (21), simply invert $\omega(t_{z_i}) = \dot{\omega}_{sec} t_{z_i} + \omega_1$ for t_{z_i} where ω_1 is an initial value. Note that this condition is valid only when perigee is secular, thus it does not apply near the critical inclination. Using the preceding condition, the potential for stationkeeping cycle instability can be predicted for a selected trajectory. This estimate, combined with the Poincaré section, can used to determine the viability of the stationkeeping method for various regions of the phase space.

Implementation Issues. Before proceeding with a discussion of the simulations, several implementation issues must be noted when applying the stationkeeping method. The attenuation factor is a design parameter that typically depends on initial conditions. A poor choice can lead to some interesting dynamics within the iteration process itself, for instance, the process may 'nearly' converge to m-iterate fixed points. Therefore, for a given orbit several damping factors should be selected to determine which provides the best convergence characteristics. An initial semi-major axis which is 'close' to other dynamical phenomena (i.e., a value near the separatrix) or a deadband that is large (i.e., a band that includes several possible dynamic responses at exact resonance) may result in a non-convergent process. As with all nonlinear dynamical systems, different initial conditions can yield a variety of responses; the stationkeeping process is in this category.

Simulations. To demonstrate these concepts, several simulations are presented. First consider a 24 hr case with a .4 eccentricity and an inclination of 23°. The Poincaré section sampled at a perigee of 270° is shown in Figure 2. The initial conditions of interest are indicated in the figure. Additionally, for the first two points (P_1 and P_2), a sketch of the resulting cycles are depicted (the cycle for P_3 is not shown for clarity). The section depicts a narrow region of chaos near the former separatrix. The remaining regions show regular orbits with libration inside the chaotic zone, and circulation outside of the zone. Because the chaotic zone is small, it is anticipated that in the majority of cases, initial conditions on the section yield a stable stationkeeping process. Selecting a deadband width of 4° and a nominal node at 75°, places the cycle nearly in the middle of the first 'lobe', P_1 in Figure 2. The initial semi-major axis is 42186.0 km, the same value that produced the invariant libration curve seen in Figure 2. From the Poincaré section, it is clear that this initial condition produces large nodal variations. To reduce this variation to lie within the deadband, the initial maneuver decreases the semi-major axis to a value near the exact resonance. The resulting cycle is near the stable fixed point, and has a long cycle length, on average 430 days, and relatively small Δv's. The semi-major axis and node history for the cycle are shown in Figure 3. The magnitude of the maneuvers has a dependence on the nominal node that is similar to the behavior observed in applying the classical method; the Δv's are smallest for λ_n near the fixed points (stable and unstable) and are largest midway between these points. Comparisons between the analytical estimates from the classical method and the numerically iterated Δv values and cycle times are shown for several node positions in Table 2. The Δv costs are average values per maneuver, where the averages are computed by taking the total cost and dividing by the total number of maneuvers in a simulation. The cycle times are computed in a similar manner by dividing the simulation time by the number of cycles.[†]

Table 2

Comparison of Average Δv per Maneuver for Several Node Positions in the 24 hr Case

$e = .4, i = 23°, \Delta\lambda = 4°$	P_1: $\lambda_n = 75°$	P_2: $\lambda_n = 120°$	P_3: $\lambda_n = 150°$
Avg. Analytical Δv (m/sec)	.116	.340	.218
Avg. Analytical Cycle Time (days)	513	175	273
Avg. Iterated Δv (m/sec)	.116	.342	.219
Avg. Iterated Cycle Time (days)	430	177	290

The results for P_1 and P_2 demonstrate the modified algorithms ability to function properly in regular regions of the phase space. Also note that the analytical predictions for the Δv costs are quite close to the

[†] The first maneuver and cycle are not included in the calculation of average values because of the large initial correction maneuver.

iterated values, however the average cycle lengths exhibit much larger variations. Furthermore, P_3 shows that it is *possible* for orbits to lie in local chaotic regions and still maintain a convergent stationkeeping process. However, the next two examples demonstrate that orbits in (local and global) chaotic regions can, quite readily, lead to divergent stationkeeping processes.

In the next simulation, a 12 hr case is selected with a .7 eccentricity and an inclination of 23°. The Poincaré section is shown in Figure 4; the figure depicts a large chaotic sea with two embedded regular regions. It is expected that stationkeeping instabilities can be encountered in this region quite readily. The selected orbit has a nominal node of 70°, a deadband width of 4°, and an initial semi-major axis of 26565 km. The initial condition and the first cycle are indicated in the section. The semi-major axis and node histories appear in Figure 5. Clearly, after the first cycle, the process encounters an instability that changes the direction of the node 'scallop'. The stationkeeping process fails; the orbit never encounters the lower boundary and leaves the vicinity of the nominal node. Also, the behavior of the semi-major axis is irregular, indicative of a chaotic response. The analytical criteria for instability in Eq. (21) predicts an action rate equal to zero (and associated sign change) at 280 days after the start of the simulation. Inspection of the node history in Figure 5 indicates an inflection point (i.e., action rate sign change) at approximately 280 days. As another example, change the inclination of the previous orbit from 23° to 55°. Increasing the inclination slows the perigee rate. This change has the effect of reducing the chaotic region to a localized neighborhood around the former separatrix, as evident in the Poincaré section shown in Figure 6. An orbit with an initial semi-major axis of 26562 km and nominal node of 100° lies directly in the chaotic region, and the resulting stationkeeping simulation is seen in Figure 7. The process continues normally for over a thousand days, however the size of the maneuvers decreases, and the slope of the semi-major axis curve during coast decreases, as well. The system is approaching an action rate equal to zero. At the start of the simulation, the analytical model predicts a zero at 1518 days, and as the simulation proceeds, the estimate improves with a final prediction of 1439 days. The figure exhibits an inflection in the node curve near 1470 days. Thus, even with local chaotic motion the possibility of stationkeeping instabilities must still be considered.

Critical Inclination. As indicated in the previous example, approach towards critical inclination slows the perigee rate to near zero, and decreases the distance between tesseral resonances. If the perigee rate is exactly zero, the tesseral harmonics would coalesce into a single resonance, thus eliminating any resonance overlap. However, at critical inclination there exists an additional resonance to consider. Since the perigee rate is near zero at the critical inclination, higher order long period zonal terms introduce a resonance between inclination and perigee. The resulting inclination/perigee phase space exhibits a resonance island similar in nature to the tesseral resonance islands. Now, because the perigee rate is never actually zero (except at isolated points), the tesseral harmonics can still interact to produce regions of chaos in the node/semi-major axis plane. Additionally, the tesserals can interact with the long-period zonals to produce regions of chaos in the perigee/inclination plane. These regions are typically local to the separatrices because the strength of the overlap is tied to the size of the perigee rate, which, at critical inclination, is extremely small. A Poincaré section depicting this behavior is shown in Figure 8. The section is the perigee/inclination plane sampled at $\lambda = 100^{\circ}$. Construction of this section proceeds slightly differently from those produced in previous examples because perigee is no longer secular. Unlike the secular case, this section is local, and depends explicitly on the selected energy (i.e., the figure depends on whether the node is librating, circulating, or chaotic). To illustrate the nature of the chaotic response at critical inclination, the selected initial semi-major axes and nodes are near the separatrices associated with the tesseral and zonal harmonics. The resulting energy level produces a chaotic section that remains local, but is larger relative to other energies.[2] Thus, as with the prior cases that have local chaos, the stationkeeping method should work properly in regular regions of the node/semi-major axis phase space that are librating, and may even work in the chaotic region. Indeed, this is the case and is depicted in Figure 9. The selected orbit is the same as in the previous simulation at i = 55°, except now i = 63.3. In this example the stationkeeping cycle remains stable throughout the simulation and lies in a locally chaotic region. A characteristic of the chaotic orbits at critical inclination is extended periods of

stable quasiperiodic motion with a sudden shift into another type of quasiperiodic motion, such as a shift from libration to circulation.

When considering only second order oblateness effects, perigee changes little even in lengthy missions. For instance, the simulation in Figure 9 is 3100 days long , and perigee changes only 25°. When luni-solar perturbations are included this result may change significantly. Analysis by Delhaise and Morbidelli[8] indicates that the period of perigee libration can decrease from a value on the order of 200 years to one near 20 years when including these effects. Their analysis also shows an increase in the size of the chaotic region. Thus, because luni-solar perturbations can have a large impact on inclination/perigee motion at critical inclination (possibly, with other inclinations and elements, as well), these perturbations should be included in further analysis of East-West stationkeeping methods for eccentric orbits.

Potential Improvements to the Method

It is desirable to improve the robustness of the stationkeeping algorithm or develop other approaches that work well in dynamically complex regions of the phase space (such as in the chaotic zones). (Initially, of course, the qualitative effects of luni-solar perturbations must be assessed to determine potential impacts to the stationkeeping algorithms.) Given the results thus far, the stationkeeping method provides stable performance if the system does not encounter an action rate equal to zero. Since the secular advance of perigee is the primary effect that produces these zeros (aside from a deadband that includes a fixed point), a candidate solution is control of perigee, thus preventing the orbit from ever encountering a zero action rate. Unfortunately, as shown in the Appendix, controlling perigee is a very 'expensive' control method for eccentric orbits. For most missions employing eccentric orbits, perigee control, as developed here, would be impractical to use as a stationkeeping strategy.

Another approach is to simply avoid placing the desired orbit in the chaotic regions. For local chaos that is isolated to small regions of phase space, this may prove sufficient for mission planning requirements. For instance, the class of orbits depicted in Figure 2 and Figure 6 has a phase space that is predominantly regular. To employ this approach, a useful mission planning tool is analytical estimates of the size of the chaotic region as a function of node and perigee. However, as the phase space becomes increasingly chaotic, such as the large sea depicted in Figure 4, avoiding these regions may be too restrictive. In such cases, an alternate or modified East-West stationkeeping method may be beneficial. A key component in the classical method is the targeting of the grazing node. This idea is predicated on the assumption that the node and semi-major axis lie in a libration region near exact resonance. Unfortunately, most of the chaotic regions also exist here. A potential alternative is to employ circulating orbits, in place of librating orbits, for targeting. The KAM Theorem guarantees that orbits sufficiently far from resonance are regular and equivalent (in the mathematical sense) to unperturbed KAM surfaces. Furthermore, simulations indicate that most circulating orbits survive tesseral perturbations. Hence, maneuvering between KAM surfaces (associated with circulating orbits and opposite nodal velocities) that surround a chaotic region, could potentially avoid the instabilities found with the present methods. The resulting orbit would form a 'box-like' drift cycle within specified deadband regions. However, this approach probably 'costs' more than the current methods because it employs two maneuvers per cycle and results in larger semi-axis variations. These strategies, and others, are currently under investigation.

Conclusions

The discussion in this paper has focused on issues relevant to East-West stationkeeping for eccentric, resonant orbits. The analysis has determined that key assumptions from classical nodal control theory break down in portions of the phase space corresponding to eccentric orbits. Namely, the node drift cycle is no longer symmetric, and a cycle's associated action rate may pass through a zero. Breakdown of the symmetry assumption introduces a numerical two point boundary value problem. Modifications to the classical theory yield an algorithm that functions properly in regions of phase space

that are similar to unperturbed libration regions (including orbits near critical inclination). However, the algorithm can fail in regions which are dynamically complex, such as in chaotic zones. The regions most susceptible to this failure can be found using Poincaré sections. Examination of the sections suggests a potential (stable) strategy is to utilize circulating orbits for targeting rather than librating orbits. The analysis in this paper has focused on the effect of tesseral perturbations, additional consideration must also be given to the impact of luni-solar perturbations. For highly eccentric orbits, these perturbations can have a significant impact on a trajectory's long-period dynamics. Alternate approaches, combined with analytical estimates that predict the size of localized chaotic regions, *may* prove useful in developing robust East-West stationkeeping strategies that can accommodate a variety of dynamic responses.

Acknowledgements

Portions of this work were supported by Purdue Research Foundation under a PRF Research Grant. The authors also wish to thank Mr. Roby Wilson for helpful technical support during this work.

References

1. Ely, T. A., and Howell, K. C. [1995]. Long Term Evolution of Artificial Satellite Orbits Due to Resonant Tesseral Harmonics. Paper No. AAS-95-196, Space Flight Mechanics Conference, Albuquerque, New Mexico.

2. Delhaise, F., and Henrard, J. [1993]. The Problem of Critical Inclination Combined with a Resonance in Mean Motion in Artificial Satellite Theory. *Celestial Mechanics and Dynamical Astronomy* **55**, 261 - 280.

3. Gedeon, G. S. [1969]. Tesseral Resonance Effects on Satellite Orbits. *Celestial Mechanics* **1**, 167 - 189.

4. Kamel, A., Ekman, D., and Tibbitts, R. [1973]. East-West Stationkeeping Requirements of Nearly Synchronous Satellites Due to Earth's Triaxiality and Luni-Solar Effects. *Celestial Mechanics* **8**, 129 - 148.

5. Chao, C., and Schmitt, D. [1989]. Eliminating GPS Stationkeeping Maneuvers by Changing the Orbit Altitude. Paper No. 89-407, AAS/AIAA Astrodynamics Specialist Conference, Stowe, Vermont.

6. Kaula, W. M. [1966]. *Theory of Satellite Geodesy*. Blaisdell.

7. Hough, M. E. [1979]. *Orbits Near Critical Inclination, Including Luni-Solar Perturbations*. Ph.D. Thesis, Stanford University, Stanford, California.

8. Delhaise, F., and Morbidelli, A. [1993]. Luni-Solar Effects of Geosynchronous Orbits at the Critical Inclination. *Celestial Mechanics and Dynamical Astronomy* **57**, 155 - 173.

9. Battin, R. H. [1987]. *An Introduction to the Mathematics and Methods of Astrodynamics*. AIAA Education Series. AIAA, New York, New York.

Appendix

'Perigee control,' as defined here, is a planar transfer between orbits that shifts the line of apsides in inertial space. The subject of optimum two-impulse transfers between two given coplanar

orbits† is addressed in a general setting by Battin.[9] He shows that a cotangential transfer orbit produces an optimum (minimum impulsive Δv's) for a 180° transfer, or for a transfer between similar points on the initial and final orbits — $v_1 = v_2 \Rightarrow r_1 = r_2$. A cotangential orbit is characterized by tangential departure and arrival at the two maneuver points. In the case of perigee control, the initial and final orbits have the same shape — their semi-major axes and eccentricities are identical. Thus, the initial and final orbits are reflected about the line of apsides of the transfer orbit. This situation is depicted in Figure 10; the departure point is labeled P_1 and the arrival point is labeled P_2. Parameters for the transfer orbit are denoted with a subscript T. When necessary, the initial orbit parameters are labeled with a subscript 1, and the final orbit with a subscript 2. However, for simplicity of notation, parameters that are the same in both initial and final orbits have no subscript.

To develop analytical conditions for the transfer orbit, several geometrical properties concerning tangent ellipses must be ascertained. First, since the transfer is symmetric, it is sufficient to consider only P_1 to uniquely determine the transfer orbit properties. The conditions at P_2 are found by reflection. Now, it is well known, that for two ellipses tangent at one point, that their empty foci and point of tangency are collinear. This fact follows directly from the focal reflection property, a fundamental geometrical property of conic sections. From this fact it follows that the distance between the empty focus on the initial orbit and the transfer orbit can be reduced to $2(a_T - a)$. Other geometrical conditions for the transfer are found easily and appear below,

$$\text{i)}\quad r = r_T \quad \Rightarrow \quad \begin{cases} \dfrac{a(1-e^2)}{1+e\cos f} = \dfrac{a_T(1-e_T^2)}{1+e\cos f_T} \\ f_T = f_1 + \dfrac{\Delta\omega}{2} \end{cases}, \tag{A.1}$$

$$\text{ii)}\quad \cos\gamma = \frac{\vec{r}_T \cdot \vec{v}_T}{r_T v_T} = \frac{\vec{r}_1 \cdot \vec{v}_1}{r_1 v_1} \quad \Rightarrow \quad \frac{e_T \sin f_T}{\sqrt{1+2e_T\cos f_T + e_T^2}} = \frac{e\sin f_1}{\sqrt{1+2e\cos f_1 + e^2}}, \tag{A.2}$$

where γ is the flight path angle and f is the true anomaly. These equations are not sufficient to uniquely specify the transfer orbit. To obtain a unique solution consider the goal of minimizing Δv; a corollary is to minimize the change in semi-major axis. From Figure 10, it is clear that a minimum value $\Delta a = a_T - a$ is achieved when the angle β between the transfer orbit's line of apsides and the line connecting the empty focus is 90°. Using this fact, the preceding conditions, and the use of planar geometry leads to the following conditions for the transfer orbit parameters, and the true anomalies corresponding to P_1 and P_2,

$$a_T = a\left(1 + e\sin\left|\frac{\Delta\omega}{2}\right|\right), \quad e_T = \frac{e\cos\left|\dfrac{\Delta\omega}{2}\right|}{e\sin\left|\dfrac{\Delta\omega}{2}\right| + 1}, \quad f_{1,2} = \mp\cos^{-1}\left[-\frac{(1+e^2)\sin\left|\dfrac{\Delta\omega}{2}\right| + 2e}{1+2e\sin\left|\dfrac{\Delta\omega}{2}\right| + e^2}\right]. \tag{A.3a,b,c}$$

The Δv can be obtained from differencing the vis-viva integral for the various orbits. A plot of Δv *per maneuver* versus the change in perigee appears in Figure 11. Except for eccentricities that are near zero, perigee control using this method does not appear feasible as a means for stationkeeping. Additionally, to apply perigee control without changing the stroboscopic node, consideration must be given to maintaining proper phasing with the Earth on the initial and final orbits, that is $\lambda_1 = \lambda_2$. This implies that the true

† Since the initial and final orbit intersect, a single impulse, non-tangential maneuver can shift the perigee, as well. However, for eccentricities below .775, this method results in higher maneuver costs than with the two-impulse approach.

anomalies in Eq. (A.3c) are most likely not the transfer points that maintain a constant node, thus perigee control combined with East-West stationkeeping costs may, in fact, cost *more* than indicated in Figure 11.

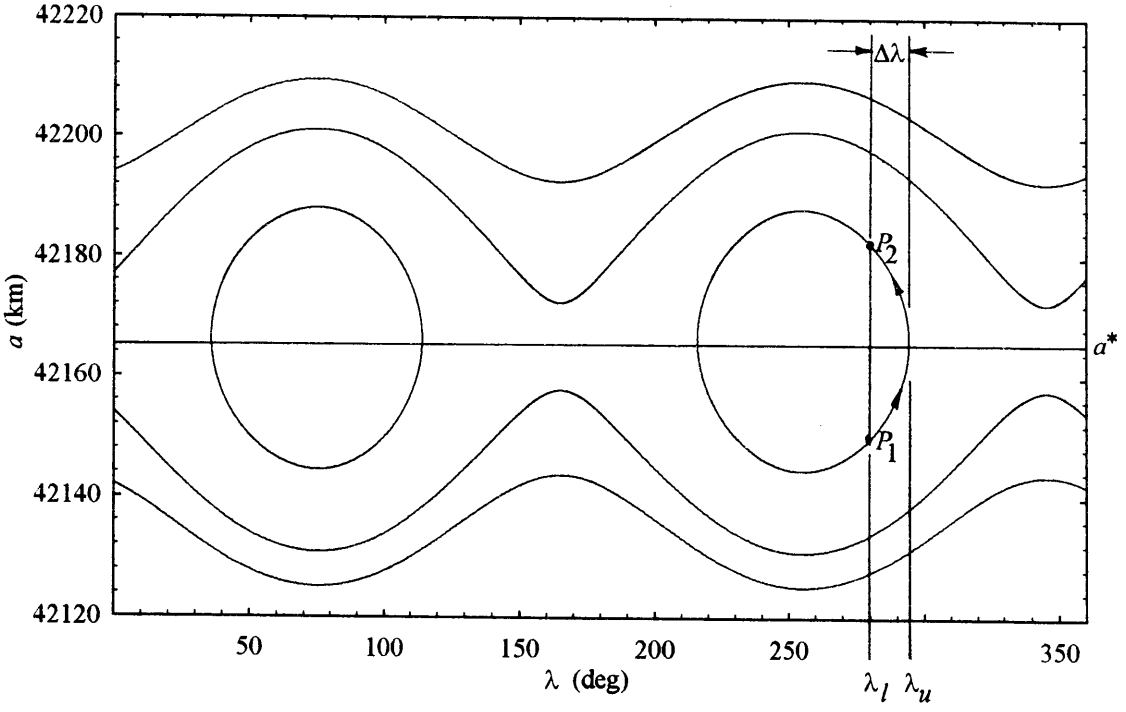

Figure 1 Phase plane: 24 hr isolated resonance ($e = 0$, $i = 0$).

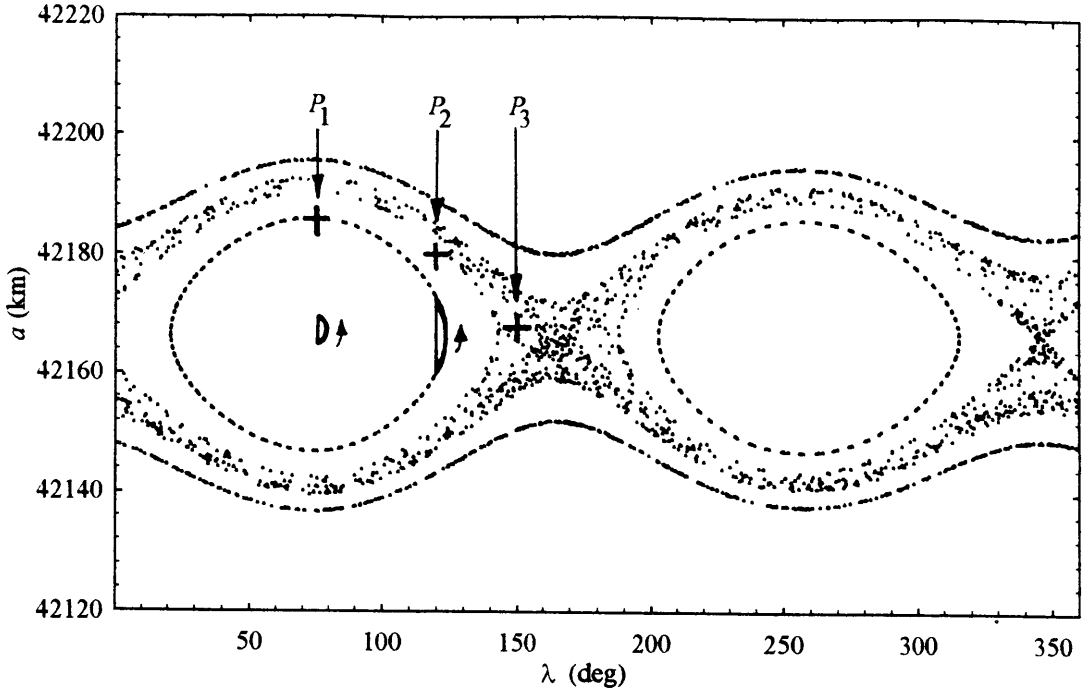

Figure 2 Poincaré section: 24 hr orbit with $\omega = 270°$ ($e = .4$, $i = 23°$).

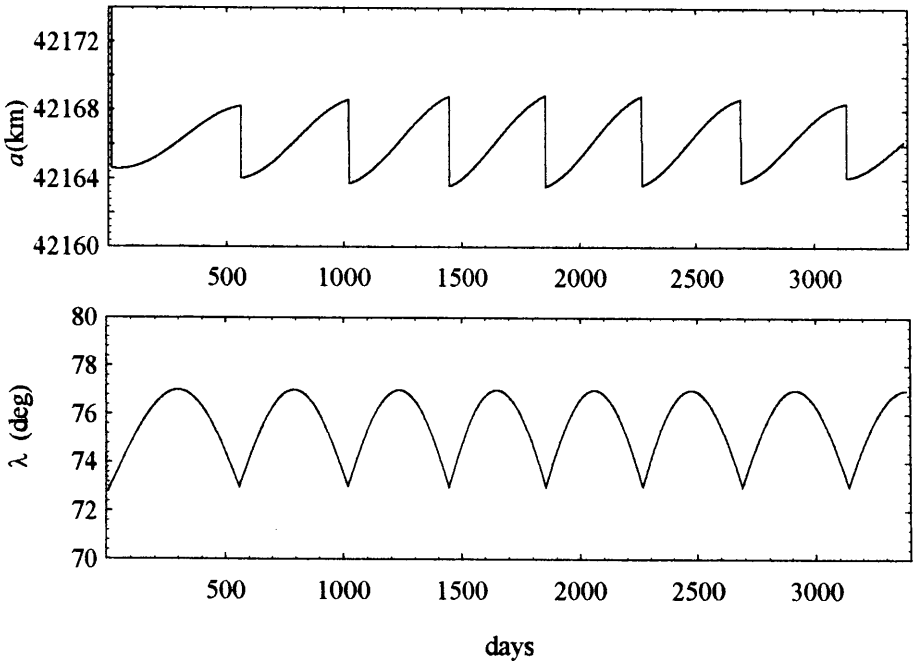

Figure 3 Stationkeeping cycle: 24 hr orbit with $\Delta\lambda = 4°$ centered at $\lambda_n = 75°$ ($e = .4$, $i = 23°$).

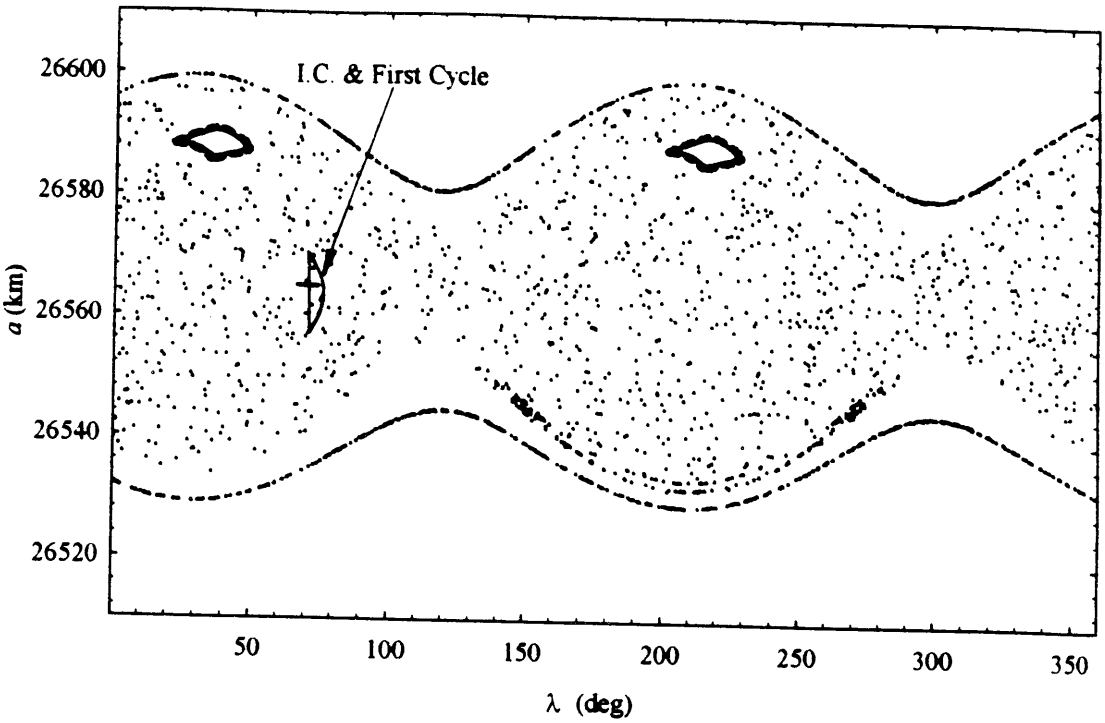

Figure 4 Poincaré section: 12 hr orbit with $\omega = 270°$ ($e = .7$, $i = 23°$).

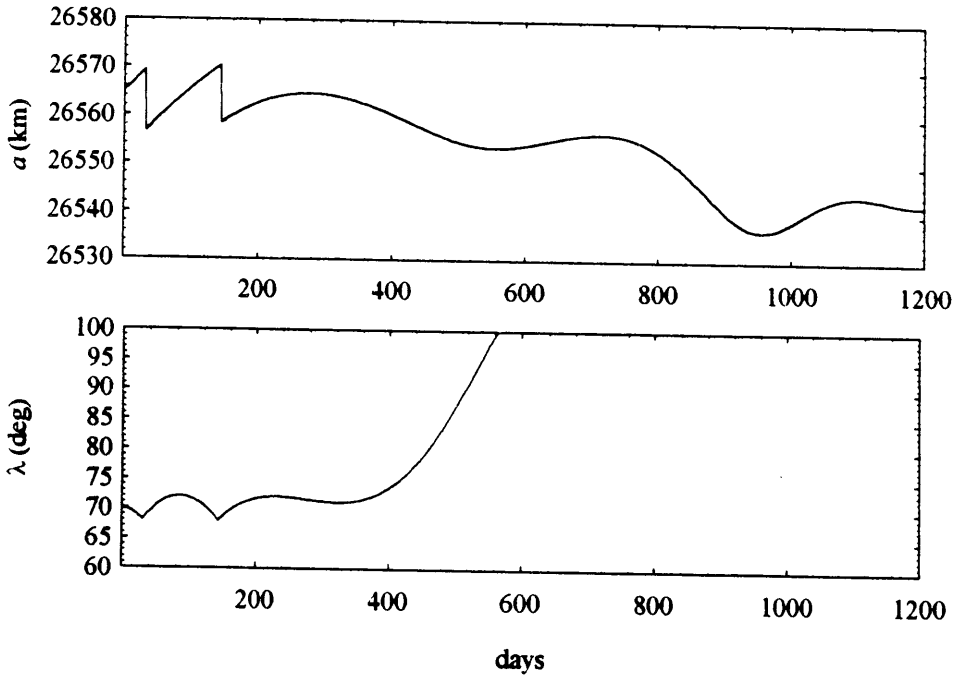

Figure 5 Stationkeeping cycle: 12 hr orbit with $\Delta\lambda = 4°$ centered at $\lambda_n = 70°$ ($e = .7$, $i = 23°$).

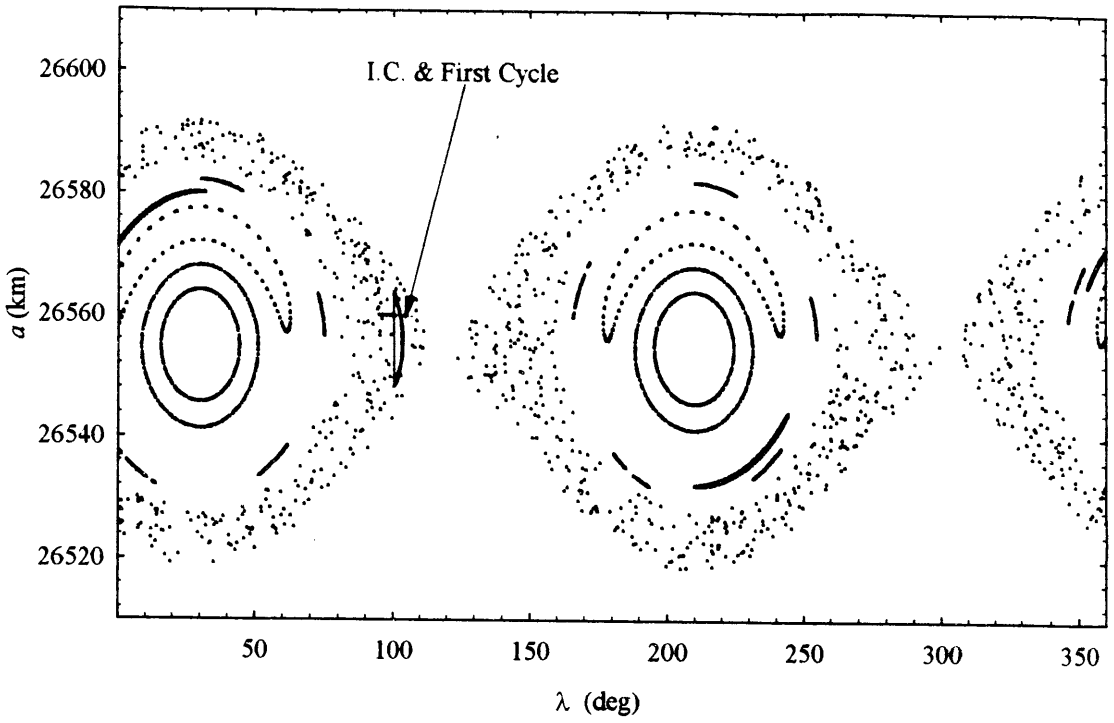

Figure 6 Poincaré section: 12 hr orbit with $\omega = 270°$ ($e = .7$, $i = 55°$).

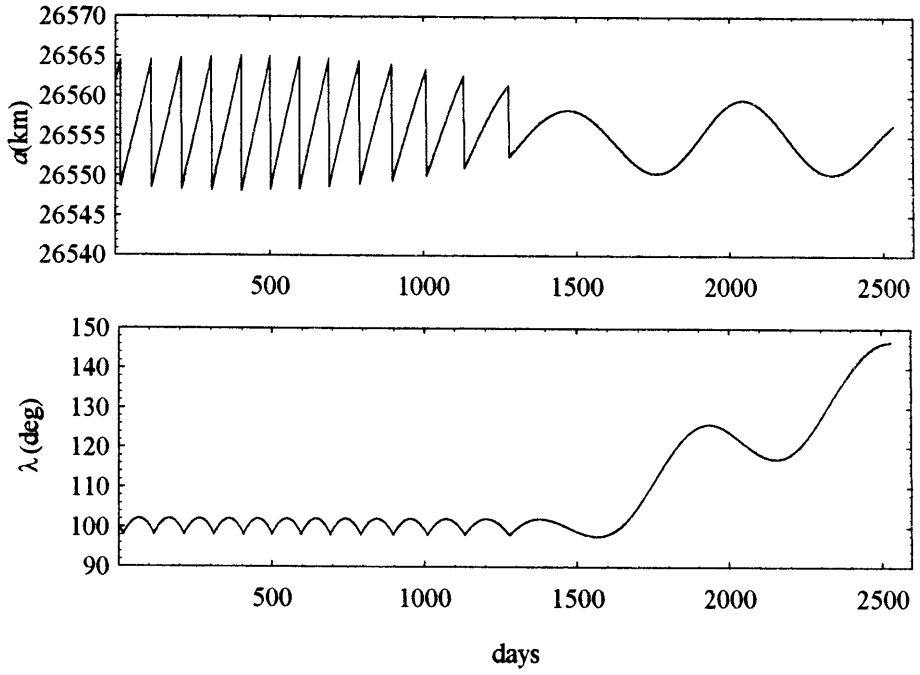

Figure 7 Stationkeeping cycle: 12 hr orbit with $\Delta\lambda = 4°$ centered at $\lambda_n = 100°$ ($e = .7$, $i = 55°$).

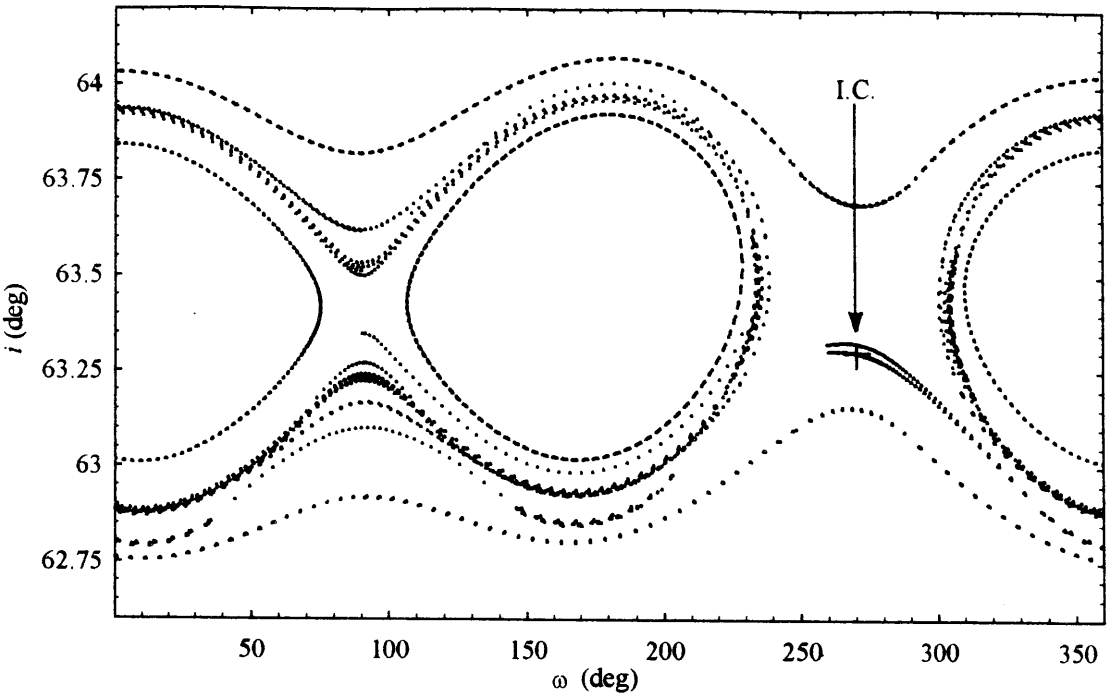

Figure 8 Poincaré section: 12 hr orbit near critical inclination with $\lambda_n = 100°$ (H = -.36018351, e = .7).

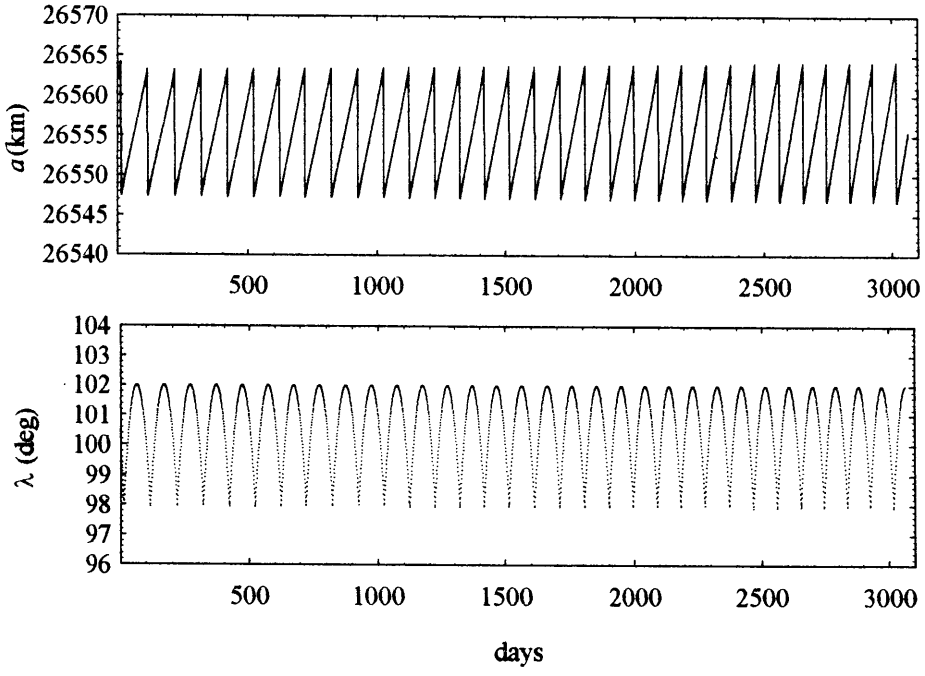

Figure 9 Stationkeeping cycle: 12 hr orbit with $\Delta\lambda = 4°$ centered at $\lambda_n = 100°$ (e = .7, i = 63.3).

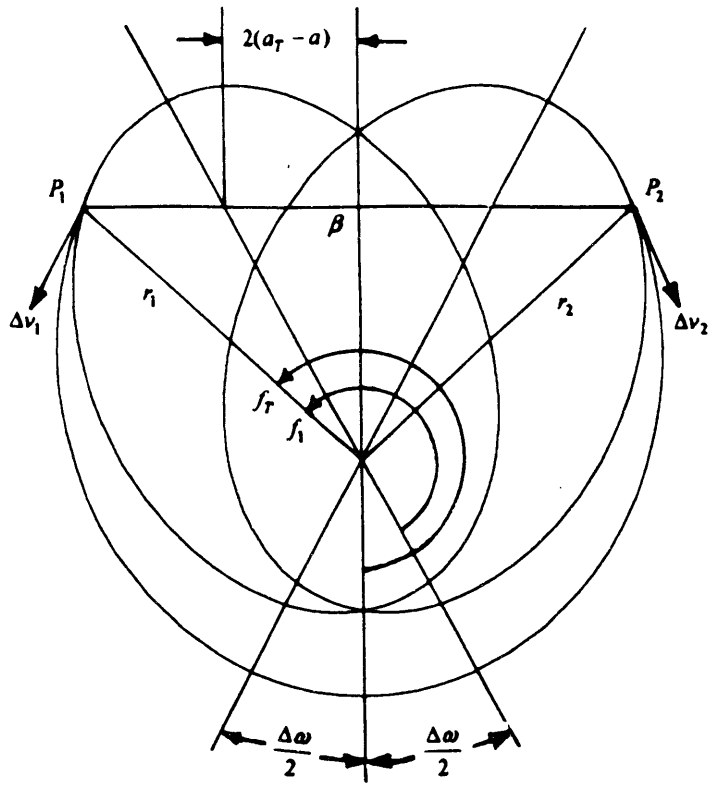

Figure 10 Initial, final, and transfer orbits for optimum perigee control.

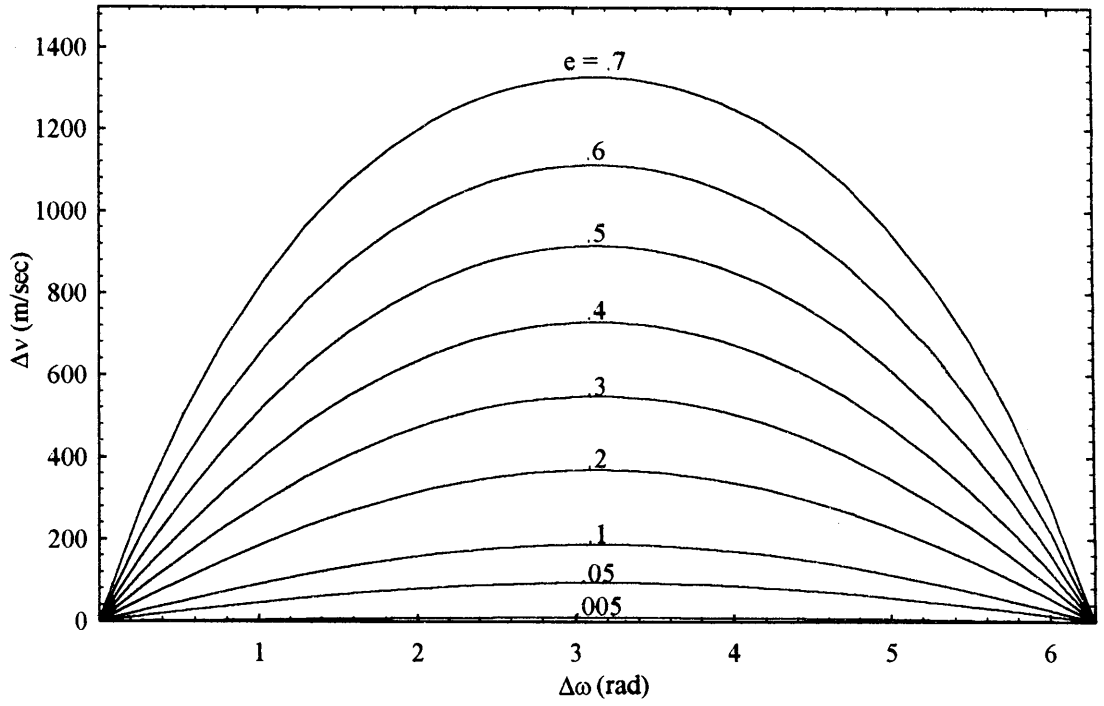

Figure 11 Cost (Δv) versus change in perigee at selected eccentricities for optimum perigee control.